



HAL
open science

Competition between electron transfer, trapping, and recombination in CdS nanorod–hydrogenase complexes

James Utterback, Molly Wilker, Katherine Brown, Paul King, Joel Eaves,
Gordana Dukovic

► **To cite this version:**

James Utterback, Molly Wilker, Katherine Brown, Paul King, Joel Eaves, et al.. Competition between electron transfer, trapping, and recombination in CdS nanorod–hydrogenase complexes. *Physical Chemistry Chemical Physics*, 2015, 17 (8), pp.5538-5542. 10.1039/C4CP05993J . hal-03546544

HAL Id: hal-03546544

<https://hal.science/hal-03546544>

Submitted on 27 Feb 2023

HAL is a multi-disciplinary open access archive for the deposit and dissemination of scientific research documents, whether they are published or not. The documents may come from teaching and research institutions in France or abroad, or from public or private research centers.

L'archive ouverte pluridisciplinaire **HAL**, est destinée au dépôt et à la diffusion de documents scientifiques de niveau recherche, publiés ou non, émanant des établissements d'enseignement et de recherche français ou étrangers, des laboratoires publics ou privés.

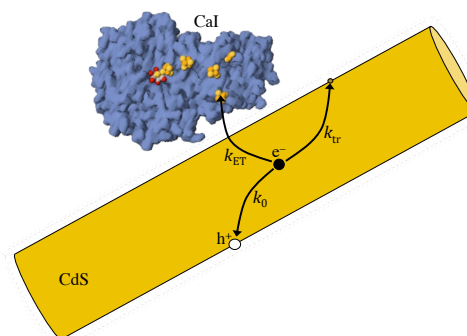
Competition between electron transfer, trapping, and recombination in CdS nanorod-hydrogenase complexes

James K. Utterback,^a Molly B. Wilker,^a Katherine A. Brown,^b Paul W. King,^b Joel D. Eaves,^a Gordana Dukovic^{*a}

Electron transfer from photoexcited CdS nanorods to [FeFe]-hydrogenase is a critical step in photochemical H₂ production by CdS-hydrogenase complexes. By accounting for the distributions in the numbers of electron traps and enzymes adsorbed, we determine rate constants and quantum efficiencies for electron transfer from transient absorption measurements.

Coupling semiconductor nanocrystals to redox enzymes is an emerging strategy to photochemically drive fuel-generating reactions such as H₂ production and CO₂ reduction.^{1–9} These hybrid structures integrate the tunable electronic structure, strong light absorption, and surface chemistry of nanocrystals with the catalytic selectivity of enzymes. Photochemical reactions of nanocrystal-enzyme complexes proceed through a sequence of steps: light absorption in the nanocrystals, transfer of photoexcited electrons to the enzyme where they participate in catalysis, and hole scavenging by sacrificial electron donors.^{2, 5, 7} The kinetics of electron transfer (ET) from the nanocrystal to the enzyme play a crucial role in the overall photochemical reactivity. The quantum efficiency of ET (QE_{ET}) determines the upper limit on the quantum yield of fuel generation. QE_{ET} , in turn, depends on how the rate of ET compares to the rates of competing excited state decay processes in the nanocrystal, such as radiative and nonradiative recombination and carrier trapping. We have recently measured electron decay kinetics in complexes of CdS nanorods (NRs) with [FeFe]-hydrogenase I from *Clostridium acetobutylicum* (CaI), which photochemically reduces 2H⁺ to H₂.² Transient absorption (TA) spectra recorded over a time window of 10⁻¹³–10⁻⁴ s indicate that ET occurs on a similar timescale as the excited state decay of NRs.² Similar results were reported in complexes of CdTe quantum dots and CaI.⁴

Quantifying the interplay between ET and the competing relaxation processes is critical for increasing the photochemical efficiency of nanocrystal-enzyme hybrids. Understanding the kinetics of nanocrystal-enzyme ET is complicated by the fact the excited states of nanocrystals decay nonexponentially over many decades in time, even in the absence of catalysts.^{10, 11, 12} These dynamics reflect the structural heterogeneities present in nanocrystal samples, some of which arise from variations in the number of carrier trapping sites on the nanocrystal surface.^{11, 13} Adsorption of enzymes further increases sample heterogeneity.¹ Average electron lifetimes in CdS NR and CdS–CaI ensemble samples can be determined from multiexponential and/or stretched exponential fits to TA data.² However, these lifetimes do not provide the intrinsic rate constants for the excited state decay processes because they do not take into account the underlying sample heterogeneity, i.e., the number distribution of electron traps and enzymes per NR in the ensemble. Thus, to understand how electron decay processes in CdS NRs compete with ET to CaI, it is necessary to use a kinetic model that accounts for population heterogeneities.



Scheme 1 Schematic depiction of photoexcited electron decay pathways in a CdS–CaI complex, including electron-hole recombination (k_0), electron trapping (k_{tr}) and electron transfer (k_{ET}).

In this communication, we employ such a model to analyze the decay of the electron population observed in the TA signal of CdS NRs and CdS–CaI complexes in the 1–100 ns time window. We determine the intrinsic rate constants, i.e. probabilities per unit time that a particular microscopic relaxation event occurs, for three electron decay processes: electron-hole recombination in CdS NRs (k_0), electron trapping (k_{tr}), and ET to CaI (k_{ET}) (Scheme 1). In this model, the numbers of the electron trap sites and adsorbed CaI moieties follow independent Poisson distributions. We find k_0 to be 1.5×10^7 s⁻¹, and k_{tr} to be 7-fold larger (1.1×10^8 s⁻¹), with the average electron trap density ($\langle N_{tr} \rangle$) of 0.59 per NR. From a series of CdS–CaI samples with varying CdS:CaI molar ratios, we find that k_{ET} (2.4×10^7 s⁻¹) is within a factor of two of k_0 . QE_{ET} in the ensemble sample is a function of both the ratios of the intrinsic rate constants and of the average numbers of traps and enzymes. While it depends strongly on the ratio k_{ET}/k_0 , the dependence on k_{tr}/k_0 is weak because $\langle N_{tr} \rangle$ is small, causing trapping to play a minor role in determining QE_{ET} for the ensemble. We find a quantitative agreement between ensemble QE_{ET} and the previously reported quantum yield of H₂ generation using CdS–CaI complexes.¹ Thus the key to more efficient photochemical H₂ generation lies in improving the efficiency of ET from CdS NRs to CaI by manipulating the individual contributions of k_{ET} and k_0 . Finally, the model predicts that the fraction of CdS NRs that have no CaI adsorbed limits the maximum achievable value of QE_{ET} for the ensemble. The kinetic model that accounts for heterogeneity of CdS–CaI complexes provides quantitative insights into factors that play a critical role in photochemical H₂ generation.

Details of the preparation and characterization of the CdS NRs and CaI have been described previously.^{1, 2} CdS NRs used in this study had an average length of 21.5 nm and an average diameter of 4.3 nm. The CdS NR surface was functionalized with 3-mercaptopropanoic acid (3-MPA), which enabled aqueous solubility and an electrostatic interaction with CaI. CaI binds to the CdS NRs via the attraction between the negatively charged carboxylate groups of deprotonated 3-MPA and a positively charged region on the surface of the enzyme

(Scheme 1).¹ This interaction is analogous to the *in vivo* binding of the electron-donating protein ferredoxin with the same positively charged region of the Cal protein surface.^{1, 5} The experimental details of sample preparation are described in Section I of the ESI†.

To monitor the relaxation kinetics of photoexcited CdS NRs with and without adsorbed Cal, we used TA spectroscopy. The laser setup has been described previously,¹⁴ and relevant experimental details are described in Section II of the ESI†. Photoexcitation of CdS NRs at 400 nm gives rise to a transient bleach feature corresponding to the band gap at 471 nm (Fig. S2, ESI†). The magnitude of the bleach is proportional to the population of electrons filling the lowest lying $1\sigma_e$ electron level of CdS NRs and is independent of the valence band hole population.^{15, 16} Thus, the decay of the bleach signal for CdS NRs without Cal represents the kinetics of electrons depopulating the $1\sigma_e$ level by radiative and nonradiative recombination with the photoexcited hole and by electron trapping. We note that Cal does not have a detectable signature in the TA spectrum at the concentrations used here.

As discussed in Section IV, ESI† and shown in Fig. S3, ESI†, the TA decay curve for CdS NRs has a complicated functional form. This is commonly observed with semiconductor nanocrystals.^{10, 17} We observe three time windows of distinct decay shapes in the relaxation of the CdS NR bleach feature. At short delay times, a fast (~ 1 ps) exponential decay component constitutes 12% of the overall decay and has recently been assigned to exciton localization.¹⁷ Most of the decay occurs in the intermediate time regime and can be fit with a stretched exponential. At long delay times (>100 ns), with the amplitude down to 2% of the initial value, the kinetics change to a much slower decay and the stretched exponential fails to describe its shape. The origin of this long-lived component remains unknown and will not be addressed here. Although the decay of the CdS NR TA signal intensity occurs over a broad range of time, most of the change in the signal intensity upon addition of Cal occurs in the window of 1-100 ns.² Thus, the 1-100 ns time regime is the most relevant for understanding ET kinetics in this system and will be the focus for the remainder of this work.

To analyze the band edge bleach recovery of CdS NRs in the 1–100 ns time window, we use a kinetic model for excited state decay that explicitly includes the number distribution of electron trap sites per CdS NR in the ensemble sample. A similar model was developed for the study of quenching kinetics of luminescent probes in micellar systems,^{18, 19} and has more recently been employed to study the kinetics of carrier trapping in nanocrystals,^{10, 20} as well as energy,^{21, 22} hole¹⁶ and electron transfer²³ in nanocrystal–acceptor complexes. The merit of this model is that it reveals the intrinsic rate constants for electron relaxation. The decay of the TA signal can be modeled as the survival probability of the electron in the $1\sigma_e$ electron state, $P_{\text{CdS}}(t)$, because $P_{\text{CdS}}(t)$ is directly proportional to $\Delta A(t)$. This model assumes that, in this time window, trapping, recombination, and ET are not dominated by diffusion. For an ensemble of NRs, $P_{\text{CdS}}(t) = \sum_{N_{\text{tr}}=0}^{\infty} P(N_{\text{tr}})P_{\text{CdS}}(t, N_{\text{tr}})$, where $P(N_{\text{tr}})$ is the probability that a NR has N_{tr} traps and $P_{\text{CdS}}(t, N_{\text{tr}})$ is the conditional survival probability for a NR that has N_{tr} traps. The model for $P_{\text{CdS}}(t, N_{\text{tr}})$ is the master equation:

$$\frac{dP_{\text{CdS}}(t, N_{\text{tr}})}{dt} = -(k_0 + k_{\text{tr}}N_{\text{tr}})P_{\text{CdS}}(t, N_{\text{tr}}). \quad (1)$$

Here k_0 is the sum of rate constants for radiative and nonradiative recombination of the electron with the hole, and

k_{tr} is the rate constant for electron trapping. At low concentrations of traps, one can find $P(N_{\text{tr}})$ using equilibrium statistical mechanics for non-interacting particles. In the grand canonical ensemble, $P(N_{\text{tr}})$ is a Poisson distribution.^{10, 24} After solving Eq. 1 and averaging over the Poisson distribution $P(N_{\text{tr}})$ (Section V, ESI†), $P_{\text{CdS}}(t)$ has the solution²⁴

$$P_{\text{CdS}}(t) = a_{\text{CdS}} \exp\{-k_0 t + \langle N_{\text{tr}} \rangle (e^{-k_{\text{tr}} t} - 1)\}, \quad (2)$$

where $\langle N_{\text{tr}} \rangle$ is the average number of traps in the ensemble. This model allows for the simultaneous determination of k_0 , k_{tr} , and $\langle N_{\text{tr}} \rangle$. In section VI of the ESI† we derive an expression that allows for fluctuations in k_{tr} at the level of second cumulant approximation, but find that they do not lead to a statistically better fit. Thus, a single value of k_{tr} is sufficient to describe the data.

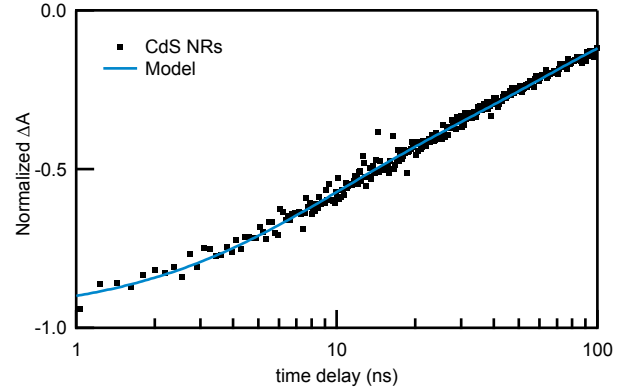


Fig. 1. TA kinetics of CdS NRs in the time window of 1–100 ns showing the fit of the kinetic model (Eq. 2) in blue.

Fig. 1 shows the TA decay of CdS NRs in the 1–100 ns time window with a fit to Eq. 2. Eq. 2 has an inherent correlation of parameters, meaning that different combinations of $\langle N_{\text{tr}} \rangle$ and k_{tr} , for example, can give the same fit. We used the bootstrapping Monte Carlo method to determine the average value and corresponding 95% confidence interval for each parameter (Section VII, ESI†). The resulting fit parameters are given in Table 1. The k_0 value of $1.5 \times 10^7 \text{ s}^{-1}$ describes electron-hole recombination pathways and is dominated by recombination of a $1\sigma_e$ electron with a surface-trapped hole because hole trapping is very fast (ps) in CdS NRs.²⁵ Electron trapping is 7-fold faster than recombination, with a rate constant of $1.1 \times 10^8 \text{ s}^{-1}$. The average number of traps is 0.59 in this sample, meaning that 33% of the NRs have one electron trap, and 55% have none. Because of the low electron trap density, the ensemble measurement of the excited state decay, and the associated average lifetime, is dominated by k_0 . Similar trapping rates and trap densities have been previously determined for CdS NRs and CdSe QDs using the same kinetic model.^{10, 24}

Table 1 Electron decay parameters for CdS NRs and CdS–Cal complexes

Cal:CdS molar ratio	k_0 (10^7 s^{-1}) ^a	$\langle N_{\text{tr}} \rangle$ ^a	k_{tr} (10^8 s^{-1}) ^a	$\langle N_{\text{Cal}} \rangle$ ^b	k_{ET} (10^7 s^{-1}) ^b
0.00:1	1.5 ± 0.1	0.59 ± 0.04	1.1 ± 0.2	–	–
0.14:1	↓	↓	↓	0.13 ± 0.02	
0.59:1	↓	↓	↓	0.42 ± 0.04	
1.14:1	↓	↓	↓	0.68 ± 0.05	2.4 ± 0.6
1.75:1	↓	↓	↓	0.76 ± 0.06	

^a Values found by fitting CdS NR kinetic trace (Fig. 1) with Eq. 2.

^b Result of global fit of data in Fig. 2 to Eq. 3 by holding k_0 , k_{tr} , and $\langle N_{\text{tr}} \rangle$ fixed, defining k_{ET} as a global parameter between data sets containing Cal and allowing $\langle N_{\text{Cal}} \rangle$ to vary between data sets.

Uncertainties associated with each fit parameter are 95% confidence intervals.

The presence of CaI introduces ET as an additional pathway by which photoexcited electrons in CdS NRs can decay. Fig. 2 shows the kinetic traces of CdS–CaI complexes with molar ratios of CaI:CdS in the range of 0.14:1 to 1.75:1. As the CaI:CdS molar ratio increases, the bleach feature of CdS recovers more quickly due to the increasing ET rate.² Mixing of CdS NRs and CaI to form complexes results in a distribution in the number of CaI adsorbed on each NR. At CaI:CdS molar ratios close to 1:1, we treat the adsorption events as independent of each other because CaI occupies a small fraction of the available surface area.¹ Thus, the number of CaI adsorbed on each CdS NR can be described by a Poisson distribution, $P(N_{\text{CaI}})$. To analyze the TA decays in Fig. 2, we use a similar treatment as described above to account for the Poisson distributions of both the electron traps and adsorbed electron acceptors. This allows us to determine k_{ET} and the average number of CaI moieties adsorbed and capable of accepting an electron, $\langle N_{\text{CaI}} \rangle$. Following a similar derivation as for $P_{\text{CdS}}(t)$ as above (Section VIII, ESI†), the TA decay of CdS–CaI complexes, $P_{\text{CdS–CaI}}(t)$, is found by averaging over both $P(N_{\text{tr}})$ and $P(N_{\text{CaI}})$.²⁴ The result is:

$$P_{\text{CdS–CaI}}(t) = a_{\text{CdS–CaI}} \exp\{-k_0 t + \langle N_{\text{tr}} \rangle (e^{-k_{\text{tr}} t} - 1) + \langle N_{\text{CaI}} \rangle (e^{-k_{\text{ET}} t} - 1)\}. \quad (3)$$

To minimize the number of adjustable parameters, the fitting of this equation to the kinetic traces of CdS–CaI complexes was performed by fixing the values of k_0 , $\langle N_{\text{tr}} \rangle$ and k_{tr} found from fitting CdS NRs alone to Eq. 2 (Fig. 1). This reflects the assumption that ET introduces another decay pathway without changing the intrinsic CdS parameters in Table 1. This assumption is supported by the fact that allowing variation in k_0 and k_{tr} upon addition of CaI does not statistically improve the fit. A global fit of Eq. 3 was performed such that recursive analysis converged upon the optimum value of k_{ET} that fits all four traces containing CaI in Fig. 2 simultaneously while allowing $\langle N_{\text{CaI}} \rangle$ to vary.

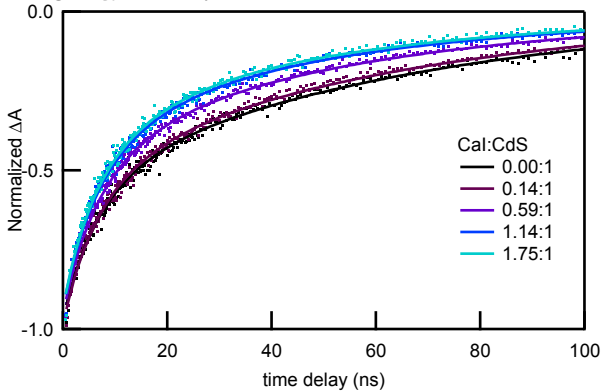


Fig. 2 TA kinetic decays of CdS–CaI complexes (points) at 470 nm for several ratios of CaI:CdS and fit functions from Eq. 3 (solid lines). The ratios listed are the mixing molar ratios during sample preparation.

The fits of Eq. 3 to the data are shown as solid lines in Fig. 2. Extracted global fit parameters for ET are given in the last two columns of Table 1. Similar values were obtained when fitting our previously published electron decay kinetics in CdS–CaI complexes using Eqs. 2 and 3 (Table S1, ESI†). Because of possible variations in the CdS NR interaction with CaI, we examined the possibility that there is a distribution in the value of k_{ET} . Using the second cumulant approximation, we included a parameter representing the variance in the values of k_{ET} . This

additional parameter did not improve the fit to the data (Section VI, ESI†). This implies that, while variations in k_{ET} may exist, they do not make a measurable contribution to the TA decays reported here.

The value of k_{ET} ($2.4 \times 10^7 \text{ s}^{-1}$) for ET from photoexcited CdS to CaI is within an order of magnitude of k_0 and k_{tr} for CdS NRs, resulting in a direct competition between these processes. While k_0 and k_{tr} are properties of CdS NRs, k_{ET} is determined by the electron pathway, which involves electron tunneling for a considerable distance from the NR surface to the distal [FeS] cluster of the enzyme.² The values of $\langle N_{\text{CaI}} \rangle$ in Table 1 increase with increasing CaI:CdS molar ratios and are consistently smaller than the mixing ratios. This observation may point to the presence of CaI adsorbed with orientations that prevent ET and/or to an equilibrium adsorption/desorption process that leaves some CaI free in solution.

For each individual CdS–CaI complex in the ensemble, competition between the processes described by k_0 , k_{tr} and k_{ET} depends on the number of traps and enzymes adsorbed (N_{tr} and N_{CaI}). For each CdS–CaI complex, $\text{QE}_{\text{ET}} = k_{\text{ET}} N_{\text{CaI}} / (k_0 + k_{\text{tr}} N_{\text{tr}} + k_{\text{ET}} N_{\text{CaI}})$. For example, in the case of a CdS NR with zero traps and one CaI adsorbed, $\text{QE}_{\text{ET}} = 62\%$, while for a NR with one trap and one CaI, $\text{QE}_{\text{ET}} = 16\%$. Note that dividing the numerator and denominator of this expression by k_0 reveals that QE_{ET} does not depend on the individual values of the intrinsic rates. Rather, it depends only on the ratios k_{ET}/k_0 and k_{tr}/k_0 .

To understand the contribution of each electron decay process to photochemical H_2 generation in solutions of CdS–CaI complexes, it is important to examine the behavior of QE_{ET} for the ensemble sample, which can be calculated by integrating $P_{\text{CdS}}(t)$ and $P_{\text{CdS–CaI}}(t)$ (Eq. S30, Section X, ESI†). For this system, QE_{ET} of the ensemble depends strongly on k_{ET}/k_0 but weakly on k_{tr}/k_0 , as shown in Fig. S6a (Section X of ESI†). To illustrate the behavior of ensemble QE_{ET} , we take the example of $\langle N_{\text{CaI}} \rangle = 1$ and calculate QE_{ET} using Eq. S30. Using the values of k_0 , $\langle N_{\text{tr}} \rangle$, k_{tr} and k_{ET} given in Table 1, the QE_{ET} would be 41%. If $\langle N_{\text{tr}} \rangle = 0$, the QE_{ET} would only increase to 43%. The small impact that trapping has on QE_{ET} reflects the fact that $\langle N_{\text{tr}} \rangle$ is already small. Increasing $\langle N_{\text{CaI}} \rangle$ above 1 would increase QE_{ET} , but this strategy decreases H_2 production, as we have shown previously.¹ H_2 generation requires transfer of two electrons to the same CaI moiety, and if multiple CaI are adsorbed on each NR, they compete for the second electron.^{1, 2} In an ensemble, there is an upper limit on the maximum achievable value of QE_{ET} , $\text{QE}_{\text{ET}}^{\text{max}}$. For a given $\langle N_{\text{CaI}} \rangle$, the fraction of NRs that do not have any CaI attached and thus do not undergo ET determines $\text{QE}_{\text{ET}}^{\text{max}}$. From Poisson statistics, the fraction of NRs with one or more CaI adsorbed is $1 - e^{-\langle N_{\text{CaI}} \rangle}$. The saturation value is therefore $\text{QE}_{\text{ET}}^{\text{max}} = 1 - e^{-\langle N_{\text{CaI}} \rangle}$. For $\langle N_{\text{CaI}} \rangle = 1$, $\text{QE}_{\text{ET}}^{\text{max}} = 63\%$. The ensemble value of 41% at $\langle N_{\text{CaI}} \rangle = 1$ achieved with the rate constants characteristic of our current system is already $\sim 2/3$ of $\text{QE}_{\text{ET}}^{\text{max}}$. A relatively modest increase in k_{ET}/k_0 by a factor of 10–100 would be sufficient to approach $\text{QE}_{\text{ET}}^{\text{max}}$ (Fig. S6b, ESI†). This could be achieved through synthetic modifications of nanocrystal surface chemistry and band structure. For example, surface-capping ligands can strongly influence ET rates from a nanocrystal to an acceptor.²⁶ Thus k_{ET} could be increased through ligand manipulation. Alternatively, type-II nanocrystals with long-lived charge separated states could decrease k_0 .^{27, 28}

Finally, we compare a previously reported value of quantum yield of H_2 generation with QE_{ET} of a corresponding ensemble sample of CdS–CaI. In our prior work, H_2 quantum yield was

20% for a CdS–CaI solution with a CdS:CaI molar ratio of 0.67.¹ Interestingly, the value of QE_{ET} with the same value of CdS:CaI, obtained by interpolating between data points in Table 1, is 21%. This similarity suggests that CaI converts electrons from photoexcited CdS NRs into H₂ with close to 100% efficiency and illustrates the remarkable electrocatalytic properties of CaI.²⁹ It also highlights the point that the key to improving H₂ production is in increasing QE_{ET} .

In summary, we have shown that a kinetic model that includes distributions in electron traps and adsorbed enzymes describes the kinetics of ET between CdS NRs and CaI in the time window of 1–100 ns. The model allows us to determine the intrinsic rate constants for electron-hole recombination, electron trapping, and ET. QE_{ET} depends strongly on the ratio of the rate constants for ET and electron-hole recombination, but only weakly on electron trapping. The maximum QE_{ET} saturates at a value determined by the fraction of NRs with no CaI moieties adsorbed. The current CdS–CaI system has a QE_{ET} value that is two-thirds of the maximum. The relatively simple model used here captures the essential kinetics of ET and provides guidance on the relevant design parameters that could be manipulated to optimize photochemical redox reactions using nanocrystal-enzyme hybrids.

CdS NR synthesis was supported by the NSF CAREER Award no. CHE-1151151 (M.B.W. and G.D.). TA measurements and kinetic modeling were supported by U.S. Department of Energy, Office of Basic Energy Sciences, Division of Materials Sciences and Engineering under Award DE-SC0010334 (J.K.U., M.B.W., G.D.). K.A.B. and P.W.K. gratefully acknowledge funding support from the U.S. Department of Energy, Office of Science, Basic Energy Sciences, Division of Chemical Sciences, Geosciences, and Biosciences; and support of the U.S. Department of Energy under Contract No. DE-AC36-08-GO28308 with the National Renewable Energy Laboratory for CaI purification, and biochemical studies.

Notes and references

^a Department of Chemistry and Biochemistry, University of Colorado Boulder, Boulder, Colorado 80309, United States. E-mail: gordana.dukovic@colorado.edu

^b Biosciences Center, National Renewable Energy Laboratory, Golden, Colorado 80401, United States.

1. K. A. Brown, M. B. Wilker, M. Boehm, G. Dukovic and P. W. King, *J. Am. Chem. Soc.*, 2012, **134**, 5627-5636.
2. M. B. Wilker, K. E. Shinopoulos, K. A. Brown, D. W. Mulder, P. W. King and G. Dukovic, *J. Am. Chem. Soc.*, 2014, **136**, 4316-4324.
3. B. L. Greene, C. A. Joseph, M. J. Maroney and R. B. Dyer, *J. Am. Chem. Soc.*, 2012, **134**, 11108-11111.
4. K. A. Brown, Q. Song, D. W. Mulder and P. W. King, *Acs Nano*, 2014, **8**, 10790-10798.
5. K. A. Brown, S. Dayal, X. Ai, G. Rumbles and P. W. King, *J. Am. Chem. Soc.*, 2010, **132**, 9672-9680.
6. C. Hamon, A. Ciaccafava, P. Infossi, R. Puppo, P. Even-Hernandez, E. Lojou and V. Marchi, *Chem. Commun.*, 2014, **50**, 4989-4992.
7. Y. S. Chaudhary, T. W. Woolerton, C. S. Allen, J. H. Warner, E. Pierce, S. W. Ragsdale and F. A. Armstrong, *Chem. Commun.*, 2012, **48**, 58-60.
8. A. Parkin, J. Seravalli, K. A. Vincent, S. W. Ragsdale and F. A. Armstrong, *J. Am. Chem. Soc.*, 2007, **129**, 10328-10329.
9. T. W. Woolerton, S. Sheard, Y. S. Chaudhary and F. A. Armstrong, *Energ. Environ. Sci.*, 2012, **5**, 7470-7490.
10. K. E. Knowles, E. A. McArthur and E. A. Weiss, *Acs Nano*, 2011, **5**, 2026-2035.
11. M. Jones and G. D. Scholes, *J. Mater. Chem.*, 2010, **20**, 3533-3538.
12. A. F. van Driel, I. S. Nikolaev, P. Vergeer, P. Lodahl, D. Vanmaekelbergh and W. L. Vos, *Phys Rev B*, 2007, **75**, 035329.
13. M. Jones, S. S. Lo and G. D. Scholes, *J. Phys. Chem. C*, 2009, **113**, 18632-18642.

14. H. W. Tseng, M. B. Wilker, N. H. Damrauer and G. Dukovic, *J. Am. Chem. Soc.*, 2013, **135**, 3383-3386.
15. V. I. Klimov, *Annu Rev Phys Chem*, 2007, **58**, 635-673.
16. J. E. Huang, Z. Q. Huang, S. Y. Jin and T. Q. Lian, *J. Phys. Chem. C*, 2008, **112**, 19734-19738.
17. K. Wu, W. Rodriguez-Córdoba and T. Lian, *J. Phys. Chem. B*, 2014, DOI: 10.1021/jp504703t.
18. P. P. Infelta, M. Gratzel and J. K. Thomas, *J. Phys. Chem.*, 1974, **78**, 190-195.
19. M. Tachiya, *Chem. Phys. Lett.*, 1975, **33**, 289-292.
20. S. Sadhu and A. Patra, *J. Phys. Chem. C*, 2011, **115**, 16867-16872.
21. G. A. Beane, A. J. Morfa, A. M. Funston and P. Mulvaney, *J. Phys. Chem. C*, 2012, **116**, 3305-3310.
22. S. Sadhu and A. Patra, *Chemphyschem*, 2013, **14**, 2641-2653.
23. A. J. Morris-Cohen, M. T. Frederick, L. C. Cass and E. A. Weiss, *J. Am. Chem. Soc.*, 2011, **133**, 10146-10154.
24. S. Sadhu, M. Tachiya and A. Patra, *J. Phys. Chem. C*, 2009, **113**, 19488-19492.
25. K. F. Wu, H. M. Zhu, Z. Liu, W. Rodriguez-Cordoba and T. Q. Lian, *J. Am. Chem. Soc.*, 2012, **134**, 10337-10340.
26. M. B. Wilker, K. J. Schnitzenbaumer and G. Dukovic, *Isr. J. Chem.*, 2012, **52**, 1002-1015.
27. S. S. Lo, T. Mirkovic, C. H. Chuang, C. Burda and G. D. Scholes, *Adv Mater*, 2011, **23**, 180-197.
28. H. M. Zhu and T. Q. Lian, *Energ Environ Sci*, 2012, **5**, 9406-9418.
29. K. A. Vincent, A. Parkin and F. A. Armstrong, *Chem Rev*, 2007, **107**, 4366-4413.

Electronic supplementary information for

Competition between electron transfer, trapping, and recombination in CdS nanorod-hydrogenase complexes

James K. Utterback,^a Molly B. Wilker,^a Katherine A. Brown,^b Paul W. King,^b Joel D. Eaves,^a and Gordana Dukovic*^a

^a Department of Chemistry and Biochemistry, University of Colorado Boulder, Boulder, Colorado 80309, USA. E-mail: gordana.dukovic@colorado.edu

^b Biosciences Center, National Renewable Energy Laboratory, Golden, Colorado 80401, USA

Table of Contents

I.	Sample preparation and characterization	S2
II.	Transient absorption (TA) spectroscopy	S2
III.	TA spectra of CdS nanorods	S3
IV.	Fitting of TA kinetics	S3
V.	The kinetic model for excited state relaxation in NRs and CdS–CaI complexes	S4
VI.	Fluctuations in both numbers and intrinsic rate constants for traps and CaI	S6
VII.	Error Analysis for k_0 , $\langle N_{tr} \rangle$, k_{tr} , $\langle N_{CaI} \rangle$ and k_{ET}	S8
VIII.	Kinetic modeling of another CdS–CaI dataset	S9
IX.	QE_{ET} as a function of the intrinsic rate constants	S10
X.	References	S11

I. Sample preparation and characterization

The synthesis of CdS nanorods (NRs) was carried out following previously reported methods.¹⁻³ UV-visible absorption spectra were recorded at room temperature in 2 mm quartz cuvettes using an Agilent 8453 spectrophotometer equipped with tungsten and deuterium lamps (Fig. S1a). The sizes of the NRs were determined by measuring over 200 particles in TEM images (Fig. S1b) using ImageJ software,⁴ giving an average length of 21.5 ± 5.2 nm and an average diameter of 4.4 ± 0.6 nm. TEM samples were made by drop casting CdS NR solution onto 300 mesh, copper grids with carbon film from Electron Microscopy Science. Images were taken using a Phillips CM100 TEM at 80 kV with a bottom-mounted 4 megapixel AMT v600 digital camera.

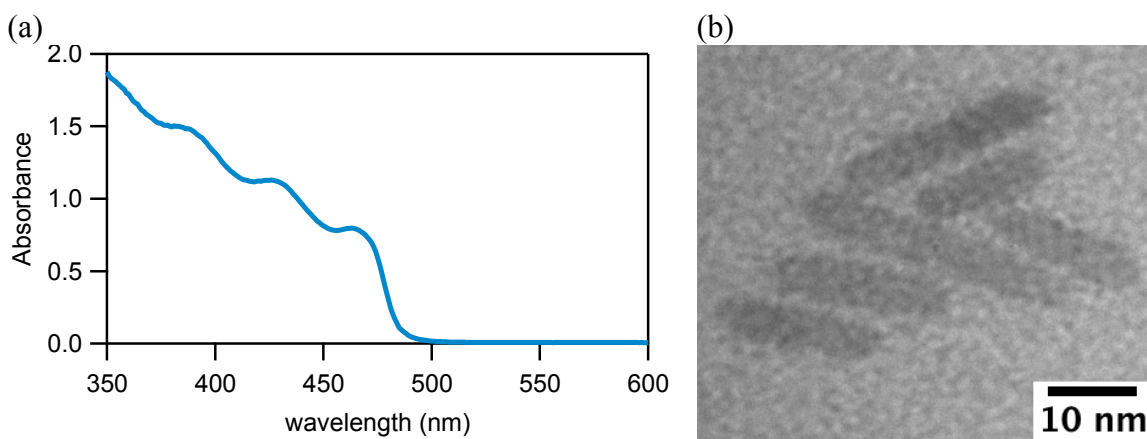


Fig. S1. (a) UV-visible absorption spectrum of CdS NRs in buffer. (b) TEM image of CdS NRs.

CdS NR surfaces were functionalized, subsequent to NR synthesis, with 3-mercaptopropanoic acid (3-MPA) using a previously reported ligand exchange procedure.^{2, 3, 5} This enabled aqueous solubility and an electrostatic interaction with CaI. The molar absorptivity of the CdS NRs was found by comparison of UV-visible absorption spectra (Fig. S1) with Cd²⁺ concentrations, found by elemental analysis (ICP-OES), after acid digestion of NR samples. The estimated molar absorptivity at 350 nm was 1.1×10^7 M⁻¹ cm⁻¹ for this sample. The expression and purification of CaI from *Escherichia coli* has been described elsewhere.⁶ CdS–CaI complexes were prepared under Ar by mixing solutions of CdS NRs and CaI in buffer (50 mM Tris-HCl, 5 mM NaCl, 5% glycerol, pH 7) with no hole scavenger added.

II. Transient absorption (TA) spectroscopy

The complete experimental setup for the TA measurements has been previously described.³ In all mixtures used for TA experiments, the concentration of CdS was held constant at about 0.7 μ M, as determined from UV-visible absorption spectra and the molar absorptivity, and the concentration of CaI was varied relative to this in order to give different molar ratios CaI:CdS. Samples were sealed under Ar in 2 mm quartz cuvettes equipped with air-tight valves. TA samples were rapidly stirred and pumped with a beam that was ~ 240 μ m in diameter with pulse energies of ~ 10 nJ. The pump power was low enough that TA decay kinetics were independent of power to prevent signal from multiple excitons⁷ and isolate the kinetics of one electron transferring to CaI. TA kinetics for data sets in Fig. 1, 2 and S5 were taken with a time resolution of 0.3 ns.

III. TA spectra of CdS nanorods

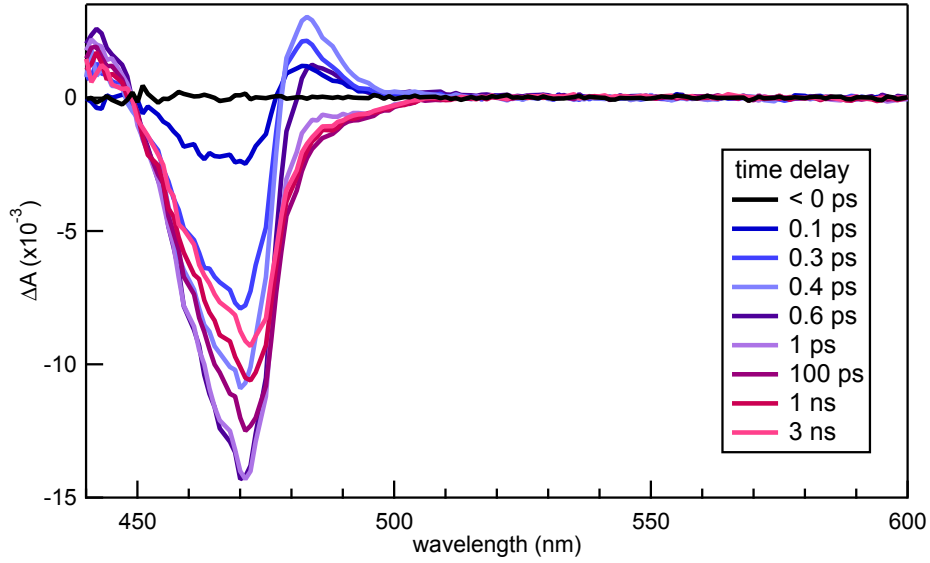


Fig. S2. TA spectra of CdS NRs after 400 nm excitation at various time delays. Photoexcitation of CdS NRs at 400 nm gives rise to a transient bleach feature peaked at 471 nm in this particular sample, corresponding the band gap. Kinetic traces are obtained by monitoring the ΔA amplitude at 471 nm. The induced absorption feature at 485 nm is due to carrier cooling and is short lived (< 1 ps).

IV. Fitting of TA kinetics

The TA decay over the time span of 0.1 ps – 30 μ s (Fig. S3) has three time windows with distinct decay shapes.

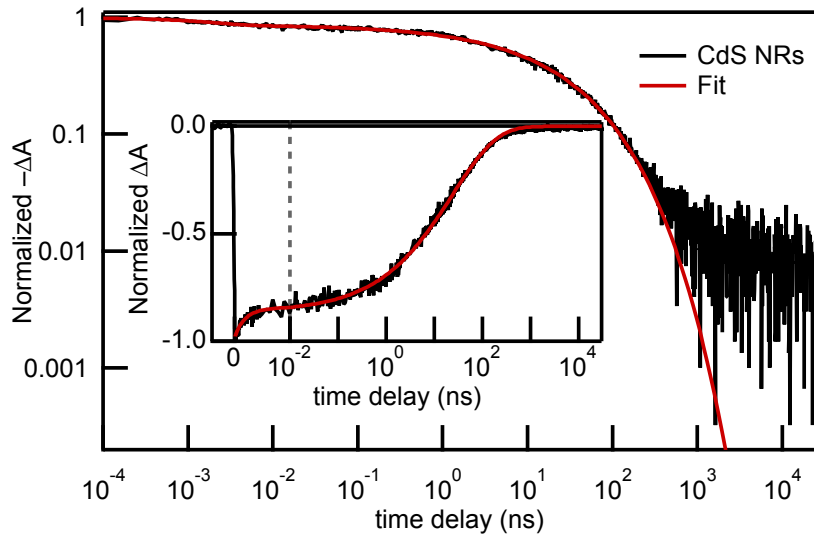


Fig. S3. TA kinetics of the band gap feature in CdS NRs probed at 471 nm over a time window of 0.1 ps–30 μ s with a time resolution of 150 fs. The signal is shown as $-\Delta A$ on log-log axes. The inset shows the same data on a split time axis that is linear for the first 10 ps and logarithmic thereafter. A fit function that includes a fast single exponential plus a stretched exponential is shown in red. The plots reveal the existence of three time windows with distinct functional forms.

The decay can be broken up into short (0.1–10 ps), intermediate (10 ps – 100 ns) and long (100 ns – 30 μ s) time windows, where each time window has a different functional

form. The single exponential plus a stretched exponential fit function used in to fit the TA band edge bleach decay of CdS NRs in Fig. S3 is

$$f(t) = A_{\text{exp}} e^{-t/\tau_{\text{exp}}} + A_{\text{stretch}} e^{-(t/\tau_{\text{stretch}})^\beta}. \quad (\text{Eq. S1})$$

The resulting fit parameters by applying Eq. S1 are $A_{\text{exp}} = -0.12$, $\tau_{\text{exp}} = 1.8$ ps, $A_{\text{stretch}} = -0.88$, $\tau_{\text{stretch}} = 24$ ns and $\beta = 0.47$. The fast 1.8 ps single exponential decay component constitutes 12% of the overall decay and has been attributed to exciton localization to a part of the nanorod with the largest diameter, or weakest quantum confinement.⁸ Most of the decay (86%) occurs in the intermediate time window and can be described with a stretched exponential with a time constant of 24 ns and a stretching exponent of 0.47. There is also a long-lived component that makes up about 2% of the ΔA amplitude that is not described by the stretched exponential fit. The origin of this component is not understood and not addressed here.

In this communication, we focus on the 1-100 ns time range because most of the TA signal change associated with ET occurs within this range.⁹ The fit to Eq. 2 produces similar parameter values to those in Table 1 when we expand the range to 0.01-100 ns.

V. The kinetic model for excited state relaxation in NRs and CdS–CaI complexes

For completeness, we present the derivation of the model of the CdS survival probability, $P_{\text{CdS}}(t)$. Though this derivation closely follows previously published works,¹⁰ it is a foundational part of our description for electronic relaxation in the presence of both traps and enzyme with and without rate constant fluctuations (Section VII).

The TA signal is proportional to the number of electrons in the $1\sigma_e$ excited state at time t , which is the survival probability of the electron in excited state, $P_{\text{CdS}}(t)$, multiplied by the total number of electrons excited at time zero. Thus the survival probability fully characterizes the time-dependent relaxation embodied in the TA signal, $\Delta A(t)$. The total survival probability, $P_{\text{CdS}}(t)$, is related to the conditional survival probability for a NR that has a given number N_{tr} of traps, $P_{\text{CdS}}(t, N_{\text{tr}})$, by the law of total probability $P_{\text{CdS}}(t) = \sum_{N_{\text{tr}}=0}^{\infty} P(N_{\text{tr}})P_{\text{CdS}}(t, N_{\text{tr}})$. Because each NR is independent, one can view $P_{\text{CdS}}(t, N_{\text{tr}})$ as the total number of electrons in the excited state at time t divided by the total number of electrons that were excited at time zero for the subpopulation where N_{tr} is fixed. $P(N_{\text{tr}})$ is the (time-independent) probability that one NR has N_{tr} traps and can be computed from equilibrium statistical mechanics. The equation of motion for $P_{\text{CdS}}(t, N_{\text{tr}})$ is the master equation,¹¹

$$\frac{dP_{\text{CdS}}(t, N_{\text{tr}})}{dt} = -(k_0 + k_{\text{tr}}N_{\text{tr}})P_{\text{CdS}}(t, N_{\text{tr}}). \quad (\text{Eq. S2})$$

The factor of $k_{\text{tr}}N_{\text{tr}}$ is the total probability, per unit time, that an electron reacts with *any* of the N_{tr} traps. The rate constant k_0 is the probability per unit time that the electron relaxes by any process other than trapping. This model assumes that the photophysics occurs in the “well-mixed” limit, i.e., that the electron samples the spatial extent of the NR on a timescale that is fast compared to the trapping time. This means that the time required for an electron to find a trap is not dominated by diffusion in this time window. The solution to Eq. S2 is

$$P_{\text{CdS}}(t, N_{\text{tr}}) = P_{\text{CdS}}(t_0, N_{\text{tr}})e^{-(k_0+k_{\text{tr}}N_{\text{tr}})(t-t_0)}. \quad (\text{Eq. S3})$$

The survival probability decays in the short time window (0.1 ps – 10 ps) in a way that is independent of N_{tr} ⁸ so that the initial condition becomes $P_{\text{CdS}}(t_0, N_{\text{tr}}) = P_{\text{CdS}}(t_0)$, the amplitude at time t_0 after the relaxation of CdS between time 0 and t_0 .

We describe the distribution of electron trap sites, $P(N_{\text{tr}})$, as an ensemble of NRs coupled to an ideal solution of traps that are noninteracting with one another but are at fixed chemical potential, temperature and volume so that the number of traps at equilibrium, N_{tr} , in a NR follows a Poisson distribution:

$$P(N_{\text{tr}}) = \frac{\langle N_{\text{tr}} \rangle^{N_{\text{tr}}} e^{-\langle N_{\text{tr}} \rangle}}{N_{\text{tr}}!}. \quad (\text{Eq. S4})$$

where $\langle N_{\text{tr}} \rangle$ is the average number of traps at thermal equilibrium. The decay of the ensemble of complexes, $P_{\text{CdS}}(t)$, computed from probability theory is then equivalent to a thermal ensemble average,

$$P_{\text{CdS}}(t) = \sum_{N_{\text{tr}}=0}^{\infty} P(N_{\text{tr}})P_{\text{CdS}}(t, N_{\text{tr}}), \quad (\text{Eq. S5})$$

$$= P_{\text{CdS}}(t_0)e^{-k_0 t} \left[\sum_{N_{\text{tr}}=0}^{\infty} P(N_{\text{tr}})e^{-k_{\text{tr}}N_{\text{tr}}t} \right], \quad (\text{Eq. S6})$$

$$= P_{\text{CdS}}(t_0) \exp\{-k_0(t - t_0) + \langle N_{\text{tr}} \rangle(e^{-k_{\text{tr}}(t-t_0)} - 1)\}. \quad (\text{Eq. S7})$$

Because $k_0 t_0 \ll 1$ and $k_{\text{tr}} t_0 \ll 1$, we simplify the fit equation by omitting t_0 and writing $P_{\text{CdS}}(t_0)$ as the amplitude, a_{CdS} :

$$P_{\text{CdS}}(t) = a_{\text{CdS}} \exp\{-k_0 t + \langle N_{\text{tr}} \rangle(e^{-k_{\text{tr}}t} - 1)\}. \quad (\text{Eq. S8})$$

This is the model (Eq. 2) we use to describe the TA decay kinetics in Fig. 1.

We arrive at Eq. 3 in the manuscript starting with a model for the conditional survival probabilities for photoexcited electrons in CdS NRs with both traps and adsorbed CaI moieties, $P_{\text{CdS-CaI}}(t, N_{\text{tr}}, N_{\text{CaI}})$. The master equation for $P_{\text{CdS-CaI}}(t, N_{\text{tr}}, N_{\text{CaI}})$ is

$$\frac{dP_{\text{CdS-CaI}}(t, N_{\text{tr}}, N_{\text{CaI}})}{dt} = -(k_0 + k_{\text{tr}}N_{\text{tr}} + k_{\text{ET}}N_{\text{CaI}})P_{\text{CdS-CaI}}(t, N_{\text{tr}}, N_{\text{CaI}}). \quad (\text{Eq. S9})$$

Just like the model discussed above, the term $k_{\text{ET}}N_{\text{CaI}}$ is the probability per unit time to decay to any of the N_{CaI} enzymes on the NR. The solution to Eq. S9 is

$$P_{\text{CdS-CaI}}(t, N_{\text{tr}}, N_{\text{CaI}}) = P_{\text{CdS-CaI}}(t_0, N_{\text{tr}}, N_{\text{CaI}})e^{-(k_0+k_{\text{tr}}N_{\text{tr}}+k_{\text{ET}}N_{\text{CaI}})(t-t_0)}. \quad (\text{Eq. S10})$$

Again, factorizing the initial conditions, $P_{\text{CdS-CaI}}(t_0, N_{\text{tr}}, N_{\text{CaI}}) = P_{\text{CdS-CaI}}(t_0)$. Assuming that the coverage of both enzymes and traps is low and that they do not interact, i.e., each is at a fixed chemical potential, the joint probability factorizes, $P(N_{\text{tr}}, N_{\text{CaI}}) = P(N_{\text{tr}})P(N_{\text{CaI}})$. Using the same model for each species as above,

$$P(N_{\text{tr}}) = \frac{\langle N_{\text{tr}} \rangle^{N_{\text{tr}}} e^{-\langle N_{\text{tr}} \rangle}}{N_{\text{tr}}!} \quad (\text{Eq. S11})$$

$$P(N_{\text{CaI}}) = \frac{\langle N_{\text{CaI}} \rangle^{N_{\text{CaI}}} e^{-\langle N_{\text{CaI}} \rangle}}{N_{\text{CaI}}!}. \quad (\text{Eq. S12})$$

Where $\langle N_{\text{CaI}} \rangle$ and $\langle N_{\text{tr}} \rangle$ are the average numbers of enzyme attached to the CdS NR and traps in the NR, respectively, at thermal equilibrium. $P_{\text{CdS-CaI}}(t)$ is therefore

$$P_{\text{CdS-CaI}}(t) = \sum_{N_{\text{CaI}}=0}^{\infty} \sum_{N_{\text{tr}}=0}^{\infty} P(N_{\text{CaI}})P(N_{\text{tr}})P_{\text{CdS-CaI}}(t, N_{\text{tr}}, N_{\text{CaI}}) \quad (\text{Eq. S13})$$

$$= P_{\text{CdS-CaI}}(t_0) e^{-k_0 t} \left[\sum_{N_{\text{tr}}=0}^{\infty} P(N_{\text{tr}}) e^{-k_{\text{tr}} N_{\text{tr}} t} \right] \left[\sum_{N_{\text{CaI}}=0}^{\infty} P(N_{\text{CaI}}) e^{-k_{\text{ET}} N_{\text{CaI}} t} \right] \quad (\text{Eq. S14})$$

$$= P_{\text{CdS-CaI}}(t_0) e^{-k_0(t-t_0)} [\exp\{\langle N_{\text{tr}} \rangle (e^{-k_{\text{tr}}(t-t_0)} - 1)\}] [\exp\{\langle N_{\text{CaI}} \rangle (e^{-k_{\text{ET}}(t-t_0)} - 1)\}] \quad (\text{Eq. S15})$$

$$= P_{\text{CdS-CaI}}(t_0) \exp\{-k_0(t-t_0) + \langle N_{\text{tr}} \rangle (e^{-k_{\text{tr}}(t-t_0)} - 1) + \langle N_{\text{CaI}} \rangle (e^{-k_{\text{ET}}(t-t_0)} - 1)\} \quad (\text{Eq. S16})$$

Again, as we did in going from Eq. S7 to Eq. S8, we replace $P(t_0)$ in favor of the amplitude, $a_{\text{CdS-CaI}}$:

$$P_{\text{CdS-CaI}}(t) = a_{\text{CdS-CaI}} \exp\{-k_0 t + \langle N_{\text{tr}} \rangle (e^{-k_{\text{tr}} t} - 1) + \langle N_{\text{CaI}} \rangle (e^{-k_{\text{ET}} t} - 1)\} \quad (\text{Eq. S17})$$

VI. Fluctuations in both numbers and intrinsic rate constants for traps and CaI

Here we derive an equation for the survival probability in the presence of fluctuations for the intrinsic rate constants. Fluctuations in the intrinsic rate constants can occur when there are additional sources of disorder in the system beyond the number fluctuations modeled above. For example, distributions in distances between the enzyme and the NR or conformational fluctuations of the enzyme might influence electron transfer rates. In this section we derive the expression for the survival probability for electron trapping when there are fluctuations in the trapping rates. Suppose there are N_{tr} traps in a NR and that the rate constant for each trap is a random variable chosen from some distribution, $k_i = k_{\text{tr}} + \delta_i$, where k_{tr} is the mean of the distribution and δ_i is the fluctuation away from the mean for a given trap, i . The distribution function for each δ_i , $p(\delta_i)$, in the set $\{\delta\} = (\delta_1, \dots, \delta_{N_{\text{tr}}})$ is identical and has finite first and second moments.

The master equation for the survival probability $P_{\text{CdS}}(t, N_{\text{tr}}, \{\delta\})$ is

$$\frac{dP_{\text{Cds}}(t, N_{\text{tr}}, \{\delta\})}{dt} = - \left(k_0 + k_{\text{tr}} N_{\text{tr}} + \sum_{i=1}^{N_{\text{tr}}} \delta_i \right) P_{\text{Cds}}(t, N_{\text{tr}}, \{\delta\}), \quad (\text{Eq. S18})$$

which is the survival probability for a given N_{tr} and a given realization of the random variable $\{\delta\}$. Solving the differential equation, and again omitting t_0 and replacing $P_{\text{Cds}}(t_0, N_{\text{tr}}, \{\delta\})$ in favor of the amplitude $P_{\text{Cds}}(t_0)$ gives

$$P_{\text{Cds}}(t, N_{\text{tr}}, \{\delta\}) = P_{\text{Cds}}(t_0) e^{-(k_0 + k_{\text{tr}} N_{\text{tr}} + \sum_{i=1}^{N_{\text{tr}}} \delta_i)t} \quad (\text{Eq. S19})$$

Because the initial condition is independent of N_{tr} , it must also be independent of the values for the intrinsic rate constants. Thus, for a given N_{tr} we can average over the fluctuations in the intrinsic rates first, and then average over the number fluctuations,

$$\langle e^{-\sum_{i=1}^{N_{\text{tr}}} \delta_i t} \rangle = \int_{-k_{\text{tr}}}^{\infty} \prod_{i=1}^{N_{\text{tr}}} d\delta_i p(\delta_i) e^{-\sum_{i=1}^{N_{\text{tr}}} \delta_i t}, \quad (\text{Eq. S20})$$

$$= \int_{-k_{\text{tr}}}^{\infty} \prod_{i=1}^{N_{\text{tr}}} d\delta_i p(\delta_i) e^{-\delta_i t}, \quad (\text{Eq. S21})$$

$$= \left[\int_{-k_{\text{tr}}}^{\infty} d\delta p(\delta) e^{-\delta t} \right]^{N_{\text{tr}}}, \quad (\text{Eq. S22})$$

$$= \hat{p}(t)^{N_{\text{tr}}}. \quad (\text{Eq. S23})$$

The simplification from Eq. S21 to Eq. S22 comes from the fact that all δ_i are independent, identically distributed random variables chosen from the same distribution. $\hat{p}(t)$ in Eq. S23 is the moment generating function for the distribution of trapping rate fluctuations, $\hat{p}(t) = \int_{-k_{\text{tr}}}^{\infty} d\delta p(\delta) e^{-\delta t}$. Finally, averaging over the Poisson distribution in N_{tr} gives the survival probability in the presence of both sources of fluctuations,

$$P_{\text{Cds}}(t) = \sum_{N_{\text{tr}}=0}^{\infty} P(N_{\text{tr}}) P_{\text{Cds}}(t, N_{\text{tr}}, \delta), \quad (\text{Eq. S24})$$

$$= P_{\text{Cds}}(t_0) \sum_{N_{\text{tr}}=0}^{\infty} P(N_{\text{tr}}) e^{-k_0 t} e^{-k_{\text{tr}} N_{\text{tr}} t} \langle e^{-\sum_{i=1}^{N_{\text{tr}}} \delta_i t} \rangle, \quad (\text{Eq. S25})$$

$$= P_{\text{Cds}}(t_0) e^{-k_0 t} e^{-\langle N_{\text{tr}} \rangle t} \sum_{N_{\text{tr}}=0}^{\infty} \frac{[\langle N_{\text{tr}} \rangle e^{-k_{\text{tr}} t} \hat{p}(t)]^{N_{\text{tr}}}}{N_{\text{tr}}!}, \quad (\text{Eq. S26})$$

which upon replacing $P_{\text{CdS}}(t_0)$ with a_{CdS} yields the final result

$$P_{\text{CdS}}(t) = a_{\text{CdS}} \exp\{-k_0 t + \langle N_{\text{tr}} \rangle (e^{-k_{\text{tr}} t} \hat{p}(t) - 1)\}. \quad (\text{Eq. S27})$$

To gauge the importance of intrinsic rate fluctuations, we approximate $\hat{p}(t)$ at the level of the second cumulant,

$$\hat{p}(t) \approx e^{\frac{\langle \delta^2 \rangle}{2} t^2}. \quad (\text{Eq. S28})$$

Including $\langle \delta^2 \rangle$ in the model functions leads to a negligible decrease in the reduced chi-square value (2% decrease) without appreciably changing the other fit parameters. Therefore, $\langle \delta^2 \rangle$ is a statistically insignificant parameter and the TA data are insensitive to fluctuations in the intrinsic rates.

A similar derivation for CdS–CaI complexes gives

$$P_{\text{CdS-CaI}}(t) = a_{\text{CdS-CaI}} \exp\{-k_0 t + \langle N_{\text{tr}} \rangle (e^{-k_{\text{tr}} t} \hat{p}_{\text{tr}}(t) - 1) + \langle N_{\text{CaI}} \rangle (e^{-k_{\text{ET}} t} \hat{p}_{\text{ET}}(t) - 1)\}, \quad (\text{Eq. S29})$$

where $\hat{p}_{\text{tr}}(t)$ and $\hat{p}_{\text{ET}}(t)$ are the moment generating functions for the distributions in trapping and ET rate fluctuations, $p(\delta_{\text{tr}})$ and $p(\delta_{\text{ET}})$, respectively.

Using the second cumulant approximation $\hat{p}_{\text{ET}}(t) \approx e^{\langle \delta_{\text{ET}}^2 \rangle t^2 / 2}$, including fluctuations in the rates for ET does not statistically improve the fit (reduced chi-squared decreases by 0.05%), indicating that a model with one representative value of k_{ET} is sufficient to describe the TA data reported here.

VII. Error analysis for k_0 , $\langle N_{\text{tr}} \rangle$, k_{tr} , $\langle N_{\text{CaI}} \rangle$ and k_{ET}

To determine the fit parameters k_0 , $\langle N_{\text{tr}} \rangle$, k_{tr} , $\langle N_{\text{CaI}} \rangle$ and k_{ET} and their uncertainties, we employed the bootstrapping Monte Carlo method.¹² Distributions for model parameters and their correlations come from generating 10,000 synthetic datasets by resampling the original data with replacement and performing nonlinear least squares fits for each set. The fit parameters that minimize the chi-square value from this process are distributed around the parameters of best fit (Table 1). Joint parameter distributions for particular pairs appear in Fig. S4.

Bootstrapping data indicate strong correlations between fit parameters as one might expect from such a nonlinear, multi-parameter data model. These correlations imply that standard error estimates of each parameter taken individually are insufficient to represent the uncertainties for all parameters simultaneously. The uncertainties reported for the fit parameters in Table 1 include covariances between parameters and represent the 95% confidence in the multidimensional parameter space.¹²

Joint probability distributions for fitting parameters

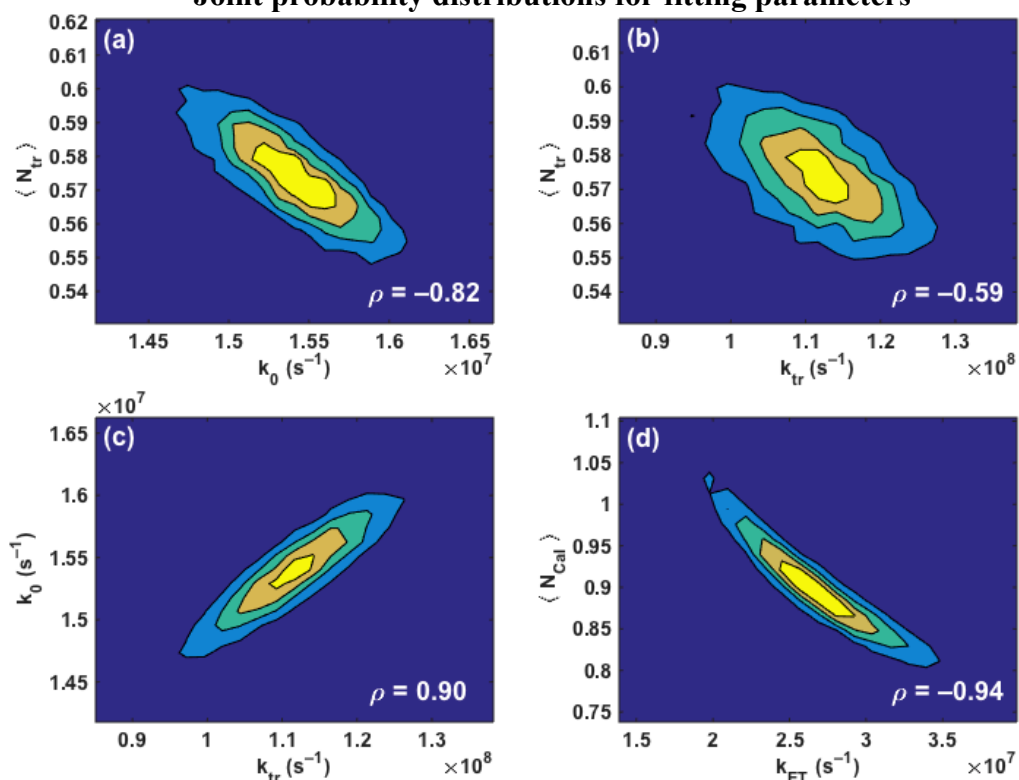


Fig. S4. Joint probability distributions for parameter pairs generated by bootstrapping Monte Carlo resampling. Parameter distributions are shown pairwise for (a) $\langle N_{tr} \rangle$ and k_0 ; (b) $\langle N_{tr} \rangle$ and k_{tr} ; (c) k_{tr} and k_0 , and; (d) $\langle N_{Cal} \rangle$ and k_{ET} . Distributions (a), (b) and (c) were produced from the 0.00:1 data set from Table S1 and (d) was produced from the 1.70:1 data set. Pearson's correlation coefficient for each pair of parameters, ρ , appears in each panel of the figure.

VIII. Kinetic modeling of another CdS-CaI dataset

To assess the reproducibility of fit parameters found in this communication, we apply our analysis to previously published data on the decay kinetics of CdS–CaI complexes.¹³ The CdS NRs used for that data set come from the same synthesis batch as the ones used in the manuscript. The fitting parameters obtained by fitting the data in Fig. S5 to Eqs. 2 and 3 are summarized in Table S1.

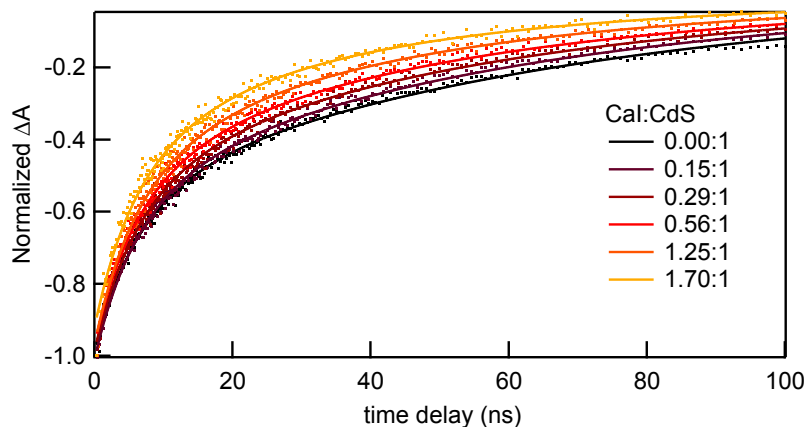


Fig. S5. Band gap TA kinetics of CdS–CaI complexes (dots) for various ratios CaI:CdS and fits to Eq. 3 of the manuscript (solid lines). Ratios listed are the molar ratios upon mixing during sample preparation.

Table S1. Electron decay parameters for another data set of CdS NRs and CdS–CaI complexes

CaI:CdS molar ratio	k_0 (10^7 s $^{-1}$) ^a	$\langle N_{\text{tr}} \rangle$ ^a	k_{tr} (10^8 s $^{-1}$) ^a	$\langle N_{\text{CaI}} \rangle$ ^b	k_{ET} (10^7 s $^{-1}$) ^b
0.00:1	1.54 ± 0.08	0.57 ± 0.03	1.1 ± 0.2	–	–
0.15:1	↓	↓	↓	0.17 ± 0.02	2.2 ± 0.3
0.29:1				0.30 ± 0.02	
0.56:1				0.44 ± 0.03	
1.25:1				0.70 ± 0.04	
1.70:1				0.99 ± 0.05	

^a Values found by fitting CdS NR kinetic trace (Fig. S5) according to Eq. 2.

^b Result of global fit of data in Fig. S5 to Eq. 3 by holding k_0 , k_{tr} , and $\langle N_{\text{tr}} \rangle$ fixed, defining k_{ET} as a global variable between data sets containing CaI, and allowing $\langle N_{\text{CaI}} \rangle$ to vary. Uncertainties associated with each fit parameter are 95% confidence intervals.

The values of k_0 , k_{tr} , and $\langle N_{\text{tr}} \rangle$ in Table S1 are consistent with those in Table 1 within the 95% confidence interval, indicating that the behavior described here is reproducible for CdS NRs made in the same synthesis. The value of k_{ET} obtained from this data set also agrees with that of the data set in the manuscript, within the confidence interval.

IX. QE_{ET} as a function of the intrinsic rate constants

While the QE_{ET} for an individual CdS–CaI complex can be calculated by $\text{QE}_{\text{ET}} = k_{\text{ET}}N_{\text{CaI}}/(k_0 + k_{\text{tr}}N_{\text{tr}} + k_{\text{ET}}N_{\text{CaI}})$, calculation of QE_{ET} for an ensemble requires the inclusion of the distribution in the number traps and adsorbed CaI. This can be done using signal intensities according to¹⁴

$$\text{QE}_{\text{ET}} = 1 - \frac{\int_0^{\infty} dt P_{\text{CdS-CaI}}(t)}{\int_0^{\infty} dt P_{\text{CdS}}(t)} = 1 - \frac{\int_0^{\infty} d(k_0 t) P_{\text{CdS-CaI}}(k_0 t)}{\int_0^{\infty} d(k_0 t) P_{\text{CdS}}(k_0 t)}, \quad (\text{Eq. S30})$$

where $P_{\text{CdS}}(t)$ and $P_{\text{CdS-CaI}}(t)$ are the fits of TA kinetics of CdS NRs to Eq. 2 and CdS–CaI complexes to Eq. 3, respectively.¹⁵ Changing integration variables in the expression for the quantum yield from t to $k_0 t$ as in the second part of Eq. S30 shows that the quantum yield of electron transfer depends only on the ratio of rate constants, so that there are two degrees of freedom and not three for fixed values of $\langle N_{\text{tr}} \rangle$ and $\langle N_{\text{CaI}} \rangle$. That is, $\text{QE}_{\text{ET}}(k_0, k_{\text{tr}}, k_{\text{ET}}) = \text{QE}_{\text{ET}}(k_{\text{tr}}/k_0, k_{\text{ET}}/k_0)$. Fig. S6a shows $\text{QE}_{\text{ET}}(k_{\text{tr}}/k_0, k_{\text{ET}}/k_0)$, evaluated by numerical integration of Eq. S30 for $\langle N_{\text{tr}} \rangle = 0.59$ and $\langle N_{\text{CaI}} \rangle = 1$. QE_{ET} shows a very weak dependence on k_{tr}/k_0 because $\langle N_{\text{tr}} \rangle$ is already very small, so the most important parameter in determining the quantum efficiency for electron transfer is k_{ET}/k_0 .

Because the most important quantity in determining QE_{ET} is k_{ET}/k_0 , increasing k_{ET} , decreasing k_0 , or changing both to increase the ratio increases the quantum efficiency for electron transfer. Fig. S6b shows the predicted values of QE_{ET} as a function of k_{ET}/k_0 , for fixed values of $\langle N_{\text{tr}} \rangle$ and k_{tr} when $\langle N_{\text{CaI}} \rangle = 1$. The circles in Fig. S6a and S6b mark the $\text{QE}_{\text{ET}} = 41\%$ calculated when the values for all parameters take on those that are measured in this communication (Table 1). QE_{ET} saturates to $\approx 63\%$ when $k_{\text{ET}}/k_0 \approx 100$. This is because at $\langle N_{\text{CaI}} \rangle = 1$, 37% of CdS NRs in the sample have no CaI adsorbed and therefore do not undergo ET.

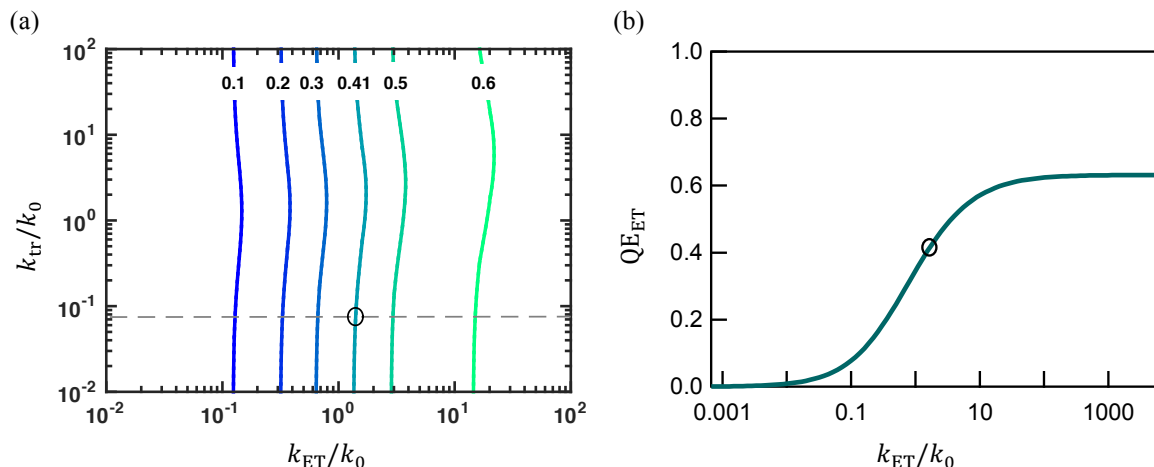


Fig. S6. Quantum efficiency of electron transfer, QE_{ET} , for $\langle N_{\text{CaI}} \rangle = 1$. (a) Contour plot of QE_{ET} as a function of k_{tr}/k_0 and k_{ET}/k_0 . Contour lines of constant QE_{ET} , where the labels denote the values of the contours, run roughly parallel to the y-axis indicating that the quantum yield for electron transfer depends very weakly on k_{tr}/k_0 when $\langle N_{\text{tr}} \rangle = 0.59$. The gray dashed line in (a) marks the slice of the data plotted in (b). The circle indicates the point in parameter space where the CdS–CaI system currently lies. $\text{QE}_{\text{ET}} = 41\%$ when k_0 , $\langle N_{\text{tr}} \rangle$, k_{tr} and k_{ET} take on the values presented in Table 1 ($k_{\text{tr}}/k_0 = 7.3$ and $k_{\text{ET}}/k_0 = 1.6$). (b) QE_{ET} as a function of k_{ET}/k_0 where k_0 , $\langle N_{\text{tr}} \rangle$ and k_{tr} values given in Table 1. This trace corresponds to the gray dashed line in (a). The circle shows the point where $\text{QE}_{\text{ET}} = 41\%$ ($k_{\text{ET}}/k_0 = 1.6$), which is the QE_{ET} we find from the fits to the TA data (Table 1).

X. References

1. P. Peng, B. Sadtler, A. P. Alivisatos and R. J. Saykally, *J Phys Chem C*, 2010, **114**, 5879-5885.
2. K. A. Brown, M. B. Wilker, M. Boehm, G. Dukovic and P. W. King, *J Am Chem Soc*, 2012, **134**, 5627-5636.
3. H. W. Tseng, M. B. Wilker, N. H. Damrauer and G. Dukovic, *J Am Chem Soc*, 2013, **135**, 3383-3386.
4. C. A. Schneider, W. S. Rasband and K. W. Eliceiri, *Nat Methods*, 2012, **9**, 671-675.
5. L. Amirav and A. P. Alivisatos, *J Phys Chem Lett*, 2010, **1**, 1051-1054.
6. P. W. King, M. C. Posewitz, M. L. Ghirardi and M. Seibert, *J Bacteriol*, 2006, **188**, 2163-2172.
7. V. I. Klimov, *Annu Rev Phys Chem*, 2007, **58**, 635-673.
8. K. Wu, W. Rodríguez-Córdoba and T. Lian, *J Phys Chem B*, 2014.
9. M. B. Wilker, K. E. Shinopoulos, K. A. Brown, D. W. Mulder, P. W. King and G. Dukovic, *J. Am. Chem. Soc.*, 2014, **136**, 4316-4324.
10. S. Sadhu, M. Tachiya and A. Patra, *J Phys Chem C*, 2009, **113**, 19488-19492.
11. N. G. VanKampen, *North-Holl Pers Libr*, 2007, 1-463.
12. W. H. Press, S. A. Teukolsky, W. T. Vetterling and B. P. Flannery, *Numerical Recipes: The Art of Scientific Computing*, 3rd edn., Cambridge University Press, 2007.
13. M. B. Wilker, K. E. Shinopoulos, K. A. Brown, D. W. Mulder, P. W. King and G. Dukovic, *J Am Chem Soc*, 2014, **136**, 4316-4324.
14. J. R. Lakowicz, *Principles of Fluorescence Spectroscopy*, Springer, New York, 2006.
15. S. Sadhu, M. Tachiya and A. Patra, *J. Phys. Chem. C*, 2009, **113**, 19488-19492.